Simulation of Gas Dynamic Behavior in Dry-Wall Inertial Fusion Energy Chambers

M. S. Tillack and N. Basu

Fusion Energy Research Program
University of California, San Diego
San Diego, CA 92093-0417

Abstract — Dry-wall chambers are currently the favored approach for laser-driven inertial fusion energy (IFE) [1]. Understanding the gas dynamic response in dry-wall chambers after a target explosion is essential in order to resolve the critical issues of chamber clearing, wall response, and propagation of targets and beams for the following shot. In order to address these critical issues, a program of experiments is anticipated in which ignition conditions will be simulated with pulsed energy sources in scaled chambers. Therefore, understanding the scaling of gas dynamic responses is critical. In this work, chamber gas dynamic responses to pulsed energy deposition were modeled numerically for different shapes, sizes and initial energy distributions in order to characterize the dependencies and to help establish the validity of size scaling for simulation experiments.

INTRODUCTION

Both modeling and experimental activities are needed to achieve a predictive capability for dry-wall laser-driven IFE chambers, particularly for the critical issues of clearing rate, wall protection, and propagation of targets and driver beams. In this work, the code TSUNAMI [2] was used to model chamber gas dynamics for different shapes, sizes and initial energy distributions, mainly to characterize the interdependencies and to establish the validity of size scaling. Previously, TSUNAMI was used primarily for studying liquid protected chambers which have a large amount of condensable vapor released after a blast [2,3]. In chambers with gas protection, the ability to achieve high repetition rate depends more on the behavior of non-condensable gases.

In the case of a gas-filled chamber, x-rays and debris from the target ignition are usually absorbed in low-pressure high-Z gas surrounding the target, resulting in a radiation-driven fireball. As a result, the gas is raised to very high temperature and pressure and expands outwards into the bulk of the chamber. Following the initial fireball, the gas undergoes repeated reflections from the boundary, and ultimately must be evacuated to prepare for the next shot. The behavior includes both subsonic and supersonic compressible flow, complicated by shock reflections from the boundaries.

The phenomena studied here include the basic response characteristics (with emphasis on the evolution towards a quiescent state) and the variation of the responses with scaling of the chamber to a smaller size and energy pulse. Multi-dimensional effects were considered essential for understanding scaling relations. Therefore, a particular case of a laser beamline was modeled to represent a more complex multi-dimensional boundary.

MATHEMATICAL MODEL

TSUNAMI solves the conservative form of Euler's equation for inviscid compressible flow in two dimensions [2]. For example, in rectangular coordinates:

$$\frac{\partial \boldsymbol{U}}{\partial t} + \frac{\partial \boldsymbol{F}^x}{\partial x} + \frac{\partial \boldsymbol{F}^y}{\partial y} = 0$$

$$\boldsymbol{U} = (\rho, \rho u, \rho v, \rho E)^T$$

$$\boldsymbol{F}^x = (\rho u,\ p+\rho u^2,\ \rho uv,\ \rho uE+up)^T$$

$$\boldsymbol{F}^y = (\rho v,\ \rho uv,\ p+\rho v^2,\ \rho vE+vp)^T$$

$$E = e + u^2/2$$

$\boldsymbol{U}$	vector of conserved quantities
$\boldsymbol{F}$	flux tensor for two coordinate system
ρ	density
u,v	velocity components in the x- and y-direction
p	pressure
E	total energy
e	internal energy

The code uses a second order extension of Godunov's method to solve the time-dependent Euler equations. The algorithm contains an explicit, upwind, conservative finite difference method.

Several important limitations may restrict the validity of the model in certain cases. For example, the gas is treated as inviscid. In order to provide a first-order estimate of the importance of viscosity, the output velocities from the code were used to estimate (by finite differencing) the magnitude of the neglected terms as compared with inertial terms in the momentum equations. In addition, the code does not account for heat nor mass transfer at the walls.

GEOMETRY AND SIMULATION PARAMETERS

The simulation parameters were chosen using Prometheus [4] and Sombrero [5] power plant designs as reference cases. When modeling small-scale chambers, the average energy density resulting from x-ray and debris deposition was preserved. For Prometheus, the total volume is 916 m^3 and the total yield is 148 MJ (31 MJ x-ray and 107 MJ debris). The volumetric energy density is thus ~150 kJ/m^3. This is the chamber averaged energy density used for all the cases

studied. The profile of energy deposition in a real IFE chamber is complex and highly design-dependent. For this work, we assumed that the energy is absorbed initially in 10% of the chamber length, and furthermore that the absorption profile could be scaled with smaller chambers. The sizes of the chambers were chosen to represent modest experimental facility sizes.

Typical IFE power plants are either cylindrical or spherical. In this work, 2D cases were studied using cylindrical coordinates to highlight multi-dimensional effects. In all cases, Xe fill gas at an initial pressure of 1 Torr and closed impermeable boundary conditions were used.

BASE CASE RESULTS

The base case is a cylindrical chamber with 1-m diameter and 2-m length. Scaling from a full-scale power plant, the energy yield in this case is 120 kJ. As a crude approximation of the energy deposition, a linearly decreasing profile in both r and z were used within 10% of the chamber nearest the center (see Figure 1). Due to symmetry, only half of the chamber was modeled in the lengthwise direction.

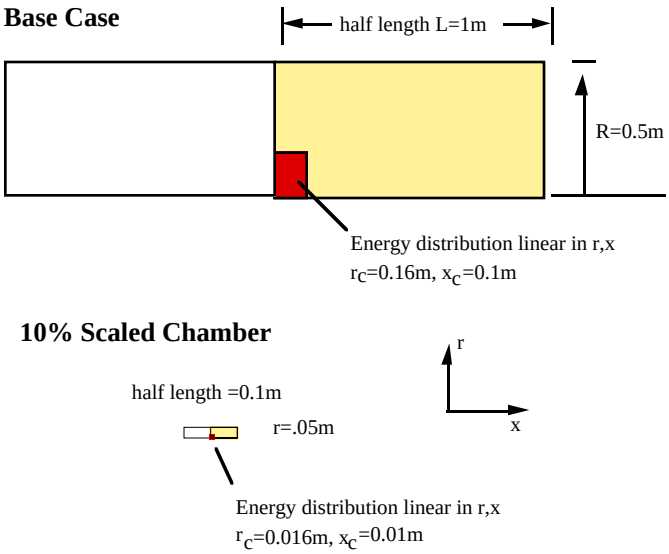

Figure 1. Cylindrical chamber geometry

The instantaneous energy deposition raises the gas to a very high pressure and temperature near the blast. This energy discontinuity forces the gas outward towards the chamber walls. Re-distribution of energy and mass in the chamber takes place by convection and is strongly affected by the chamber geometry. Initially all of the energy is in the form of internal energy, which is eventually converted partly to kinetic energy.

Figures 2–4 show plots of pressure with time at different locations in x (at r=0.25 m) and r (at x=0.5 m) for the base case. These plots show the initial expansion from the center and reflection from the boundary. On the return path, convection is impeded by gas which is still flowing outwards. In addition, the temperature begins to decrease, resulting in a lower sound speed. The ensuing velocity profiles are farily complex. After a few oscillations (beyond ~0.5 ms), mixing of reflections off of the various walls eventually results in a periodically varying state with reduced amplitude.

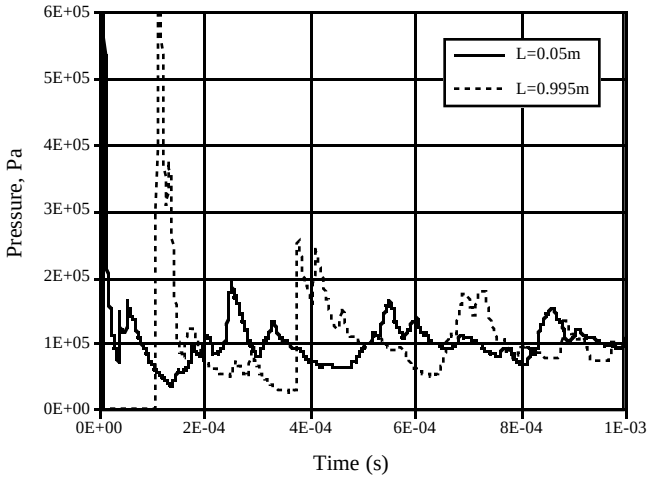

Figure 2. Base case pressure history at r=0.25 m

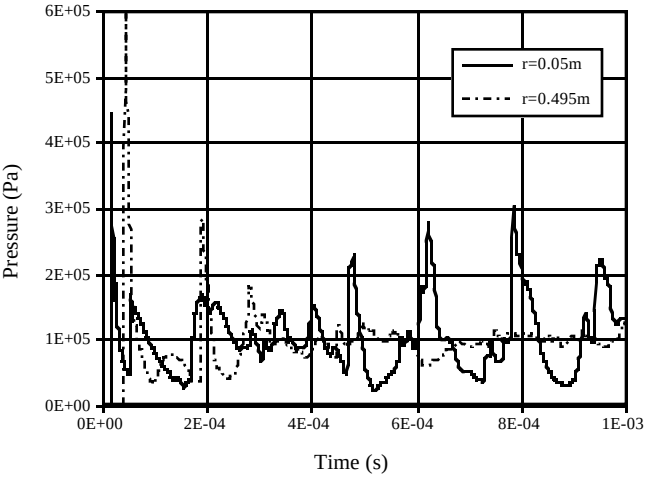

Figure 3. Base case pressure history at x=0.5 m

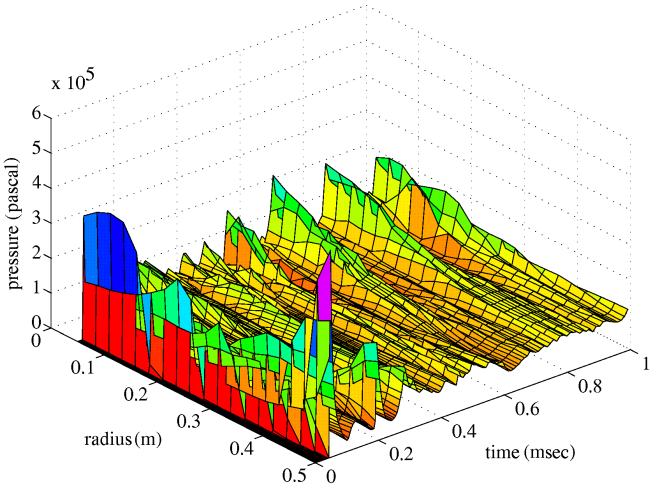

Figure 4. Base case pressure *vs.* time at x=0.5 m

As shown in Figure 2, the initial shock reaches the wall at x=L at ~0.1 ms (for r=0.25 m). The discontinuity is reflected from the wall, propagates back towards the origin and gets reflected again due to a similar pulse coming from the opposite direction. It reaches the x=L wall again at ~0.37 ms, indicating a slowing of the average velocity. The finite spatial extent of the initial energy distribution adds an additional layer of complexity and moderates the sharpness of the response.

As shown in Figures 3 and 4, the pulse reaches the wall at r=R in approximately half the time as the axial wall. The peak pressure is higher near the axis as a result of the 1/r convergence. The radial and axial reflections take place at different times, which results in convective mixing and redistribution of energy and mass in the chamber. Eventually, a semi-quiescent state is reached in which the pressure changes in a periodic manner.

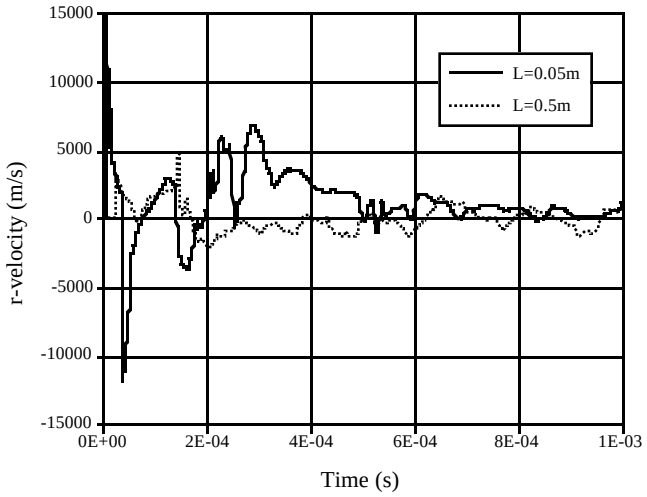

Figure 5. Velocity history at r=0.25 m

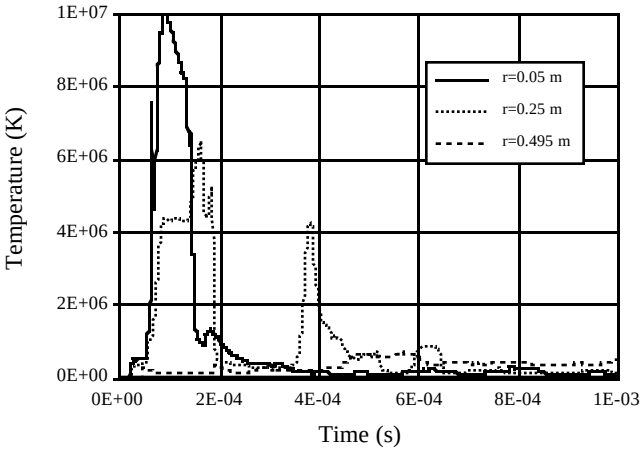

Figure 6. Temperature history at r=0.25 m

Figure 5 shows the radial component of velocity at r=0.25 m. An initial velocity excursion to 15~20 km/s occurs near the midplane following the addition of energy to the gas, but on average the convective velocity is of the order of 2000 m/s. Comparing the convective speed with the sound speed is very difficult, due to the strong spatial and temporal variation of temperature and density. Careful comparison of Figure 5 with Figure 2 shows that the velocity and pressure correlate to some extent, but the pressure excursions result from both convective flows as well as shocks traversing the chamber.

Figure 6 shows the temperature history corresponding with Figure 2. Since radiation opacities and transport in this high-temperature regime are not modeled accurately in TSUNAMI, the resulting temperatures should be viewed qualitatively.

SCALED CHAMBERS AND VISCOUS EFFECTS

Results were obtained for a chamber with both the dimensions and the initial energy profile scaled by 10%, and with energy input of 120 J instead of 120 kJ. The pressure and velocity responses are exactly identical to those shown in Figures 2–4, except that the time scale is reduced by a factor of 10 for the smaller chamber. For this case, the key question is whether dissipative mechanisms – *e.g.*, viscosity and heat transfer – will result in size scaling effects.

A first order estimate was made *a posteriori* by comparing the magnitude of the viscous terms in the full momentum equations with the inertial terms using the velocity profiles computed from the Euler equations. Figure 7 shows a sample result of the ratio of viscous to inertial terms at 0.9 ms for the base case as a function of x and r. Since the inertial term can vanish at any given location and time, the ratio can be large locally. However, on average, the viscous term is less than 1% of the inertial terms, with a peak of only ~3%.

In the smaller chamber, the ratio of viscous to non-viscous terms is larger by exactly the scaling factor of 10. This is due to the fact that the velocity gradient arising from the energy discontinuity increases when the chamber is scaled to a smaller size, keeping the volumetric energy density and mass density of the chamber constant.

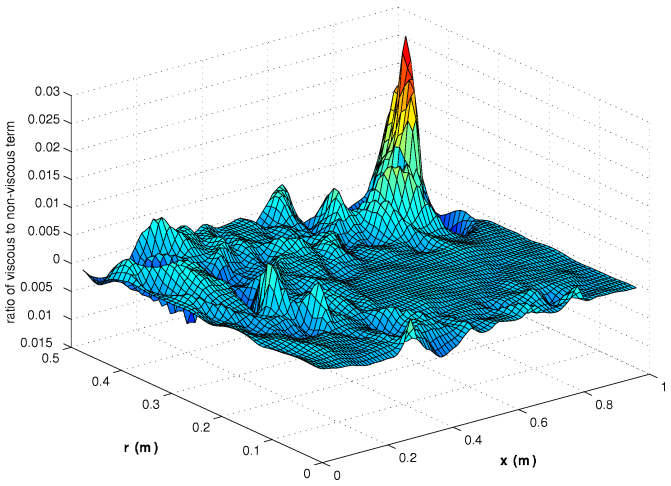

Figure 7. Ratio of viscous to inertial terms for Case I (v_x in x momentum equation at 0.9 ms)

BEAMLINE EFFECTS

A laser beamline was simulated in order to examine the effect of complex geometry, as shown in Figure 8. The addition of the beam line causes both an additional source of reflections and also a large "sink" into which gas can flow, accumulate and then return into the main chamber.

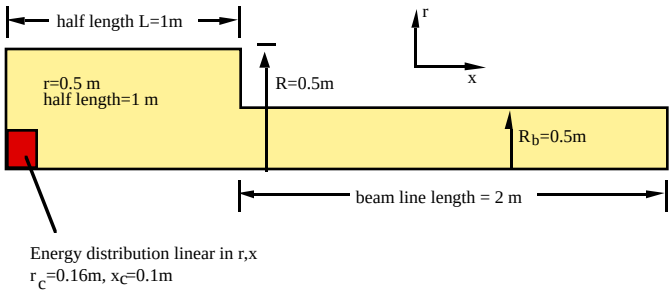

Figure 8. Geometry of cylindrical chamber with beamline

Comparing Figure 9 with Figure 3, the early behavior is very similar. The most notable difference is in the reduction of peak pressure near the axis following the reflection at 0.6 ms. Using the results from the base case, one would expect the first response from the end of the beam line to return to the main chamber after 0.5–1 ms. The effect of the return gas flow apparently is to "sweep away" the radial oscillations and cause a more rapid calming of the chamber.

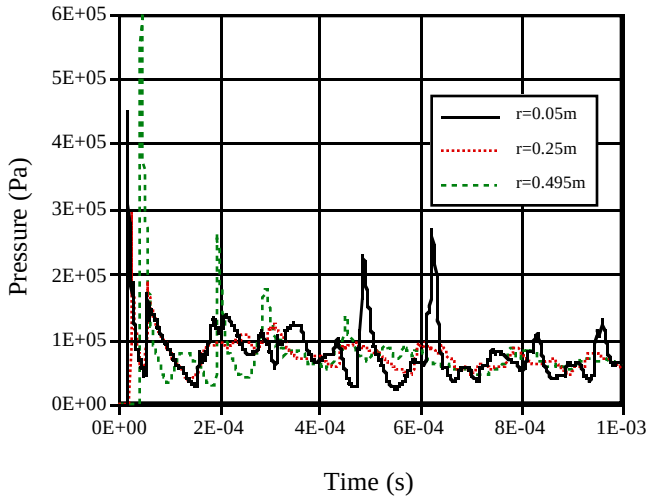

Figure 9. Pressure histories at x=0.5 m for the beamline case

CONCLUSIONS

The gasdynamic response of cylindrical chambers has been analyzed using the TSUNAMI computer model. Initial energy distributions were used to approximate the conditions in the gas immediately following a target explosion. The overall responses were explored, with particular emphasis on the time required to reach quiescent conditions. The effect of scaling was studied in order to determine whether small-scale simulation experiments might be used in order to better understand the responses in reactor-relevant chambers.

1) Overall character of the response. The gasdynamic response in chambers with relatively low initial gas density is characterized by strong convective flows emanating from the high initial pressure created by localized absorption of the blast energy. Following the initial outward expansion, the gas reflects off of the chamber walls and begins to interact with its own reflections. The flow patterns quickly reach a chaotic state, after which a low-level oscillation persists. This oscillation continues over long periods of time due to the absence of dissipative forces. This semi-quiescent state is reached within milliseconds.

2) Effect of size scaling. If the initial energy is scaled proportionally with the volume and the distribution of energy remains similar, then the pressures and velocities in scaled chambers closely match those of larger chambers. The primary difference is that the time scale is proportionally reduced with the scale length.

3) Neglect of viscosity, heat and mass transfer. *A posteriori* evaluation of the viscous terms in the full momentum equation shows that their magnitude is small compared with inertial terms in the initial stages of the chamber gas response. The relative importance increases as the chamber size decreases.

The calculations also neglected both heat and mass transfer at the walls. The computed temperatures are therefore conservative, since radiation and conduction are neglected. Lower temperatures would result in lower pressures, but would not likely affect the number density.

4. Beamline effects. The addition of a beam line reduced the peak of the pressure pulse by creating additional reflections and by the accumulation of mass in the beam lines.

REFERENCES

[1] B. G. Logan, *et al.*, "Progress and Critical Issues for IFE Blanket and Chamber Research", 5th Intl. Symposium on Fusion Nuclear Technology, Rome, Sept. 1999, to be published in *Fusion Engineering and Design*.

[2] X. M. Chen, V. E. Schrock, P. F. Peterson, "Gas Dynamics in the Central Cavity of the HYLIFE-II Reactors," *Fusion Technology* **21** (1992).

[3] J. C. Liu, "Experimental and Numerical Investigations of Shock Wave Propagation Through Complex Geometry, Gas Continuous, Two-Phase Media," UC Berkeley Ph.D. thesis, UCRL-116871, 1993.

[4] Inertial Fusion Energy Reactor Design Studies, Prometheus-L and Prometheus-H Final Report," DOE/ER-54101, MDC 92E0008, March 1992.

[5] W. R. Meier, *et al.*, "OSIRIS and SOMBRERO Inertial Fusion Power Plant Designs: Final Report," WJSA-92-01 (DOE/ER/54100-1) March 1992.